Journal of The Electrochemical Society, **161** (3) F318-F322 (2014)
0013-4651/2014/161(3)/F318/5/$31.00 © The Electrochemical Society

Influence of the RuO_2 Nanosheet Content in RuO_2 Nanosheet-Pt/C Composite Toward Improved Performance of Oxygen Reduction Electrocatalysts

Christophe Chauvin,* Takahiro Saida,* and Wataru Sugimoto*,z

Faculty of Textile Science and Technology, Shinshu University, Ueda, Nagano, 386-8567 Japan

A series of composite electrocatalysts composed of RuO_2 nanosheets and carbon supported Pt (RuO_2ns-Pt/C) has been synthesized by mixing different amounts of commercial 50 wt% Pt/C with RuO_2ns derived from exfoliation of layered $K_{0.2}RuO_{2.1} \cdot nH_2O$. The oxygen reduction activity and stability of the different electrocatalysts has been evaluated as a function of the nanosheet content in the composite electrocatalysts. An increase in initial activity was observed for composite electrocatalyst with RuO_2/Pt<0.4. After conducting accelerated durability tests, the RuO_2ns-Pt/C composite electrocatalyst with RuO_2/Pt = 0.3 exhibited a 25% higher mass activity toward oxygen reduction than the pristine Pt/C electrocatalyst.
 [DOI: 10.1149/2.077403jes]

Manuscript submitted November 20, 2013; revised manuscript received December 27, 2013. Published January 7, 2014. This was Paper 1366 presented at the Honolulu, Hawaii, Meeting of the Society, October 7–12, 2012.

Carbon supported platinum and platinum-based alloy electrocatalysts are commonly used for the cathode catalyst in polymer electrolyte membrane fuel cells.[1] Improved initial electrocatalytic activity and suppression of loss in electrocatalytic activity during fuel cell operation are major obstacles that must be overcome for wide-spread commercialization. It has been suggested that alloys such as Pt with Co, Ru, Fe, Cr or Ni lead to higher oxygen reduction reaction activity due to favorable Pt-Pt distance, electronic structure or Pt crystal orientation.[2–12] Unfortunately, the promoter metal can often easily dissolve from the alloy leading to loss in catalytic activity[13] and in some cases damage the polymer electrolyte membrane.[14]

One way to overcome these drawbacks is to use electrochemically stable oxides as additives. Some metal oxides have been suggested to help oxygen dissociation, promote interaction with Pt, and improve the ionic mobility.[15,16] Metal oxide supported Pt electrocatalyst based on TiO_2, SnO_2, RuO_2 or TiO_2-RuO_2 have also been developed.[17–20] While most of these composite electrocatalysts show improved durability compared to Pt/C, very few of these electrocatalyst show higher or even comparable initial activity. RuO_2 is one of the few oxides that is an exception, possessing good electronic conductivity and high electrochemical stability within the hydrogen and oxygen evolution region.[21,22] The addition of RuO_2 has been shown to increase the activity toward oxygen reduction by improving the wettability of the catalyst layer due to self-humidification.[23–25] The addition of RuO_2 has also been reported to catalyze the oxidation of water, therefore providing protection from other redox active species at high cathode potential.[26] An enhancement in the electronic structure through interaction between Pt and RuO_2 has also been suggested.[27]

We have reported the use of RuO_2 nanosheets (RuO_2ns) with thickness of ∼1 nm as an efficient co-catalyst.[22,28] RuO_2ns has been shown to enhance activity and durability of Pt/C as an anode[29,30] as well as cathode catalyst.[31] In an earlier study, it was shown that the durability of commercial Pt/C (20 mass% of Pt) with ultrasmall Pt (1–1.5 nm) could be improved without sacrificing initial activity.[32] Smaller nanoparticles generally have higher rate of dissolution[33] and thus are not commonly considered for practical fuel cells.

In this study, a commercial Pt/C electrocatalyst (50 mass% Pt, particle size ∼3 nm), a common cathode catalyst with high mass activity for the oxygen reduction reaction (ORR), was used to prepare a series of RuO_2ns-Pt/C composite electrocatalyst with different RuO_2ns content, and the effect of the RuO_2ns content toward initial activity and catalyst durability has been studied.

Experimental

Electrocatalyst preparation and characterization.— The RuO_2ns aqueous colloid was obtained by a process described previously.[28] Briefly, the interlayer K^+ cation in the layered $K_{0.2}RuO_{2.1} \cdot nH_2O$ was exchanged with H^+ by acid treatment with 1 M HCl. The resulting layered $H_{0.2}RuO_{2.1} \cdot nH_2O$ powder was added to a solution of aqueous tetrabutylammonium hydroxide and shaken for 10 days. The product was centrifugated at 2000 rpm for 30 min to remove any non-exfoliated material. The colloidal suspension, which contains exfoliated, monolayered RuO_2 nanosheets, was used for further experiments.

Pt/C powder (TEC10E50E, Tanaka Kikinzoku Kogyo, 50 mass% Pt, particle size ∼3 nm) was dispersed in ultrapure water by stirring and ultrasonification. Aqueous RuO_2ns colloid (1 mg-RuO_2 mL^{-1}) was slowly dropped into the Pt/C dispersion (5 mg-Pt/C mL^{-1}) under continuous stirring. The amount of colloid was tuned so as to obtain catalyst composition with molar ratio of RuO_2:Pt = n:1, where n = 0.05, 0.1, 0.2, 0.3, 0.4 and 0.5. After further magnetic stirring and ultrasonification to ensure homogeneous reaction, the powder was collected, washed until neutral pH with ultrapure water and then dried overnight at 120°C to a powder state. Homogeneous reaction between RuO_2ns and Pt/C is evident by sedimentation after allowing the mixed suspension to stand for a few hours, coupled with a change in the color of the solution from black to transparent. Both RuO_2ns and Pt/C are individually stable for this period of time. The composite electrocatalysts will be abbreviated as RuO_2ns(n)-Pt/C, where n is the RuO_2/Pt ratio.

The structure of the electrocatalyst was characterized by X-ray diffraction (XRD, Rigaku RINT 2550 with monochromated CuKα radiation). The morphology of the electrocatalyst was observed by scanning electron microscopy (SEM, Hitachi S5000) and transmission electron microscopy (TEM, JEOL JEM2010).

Catalyst ink and electrode preparation.— The catalyst ink was prepared by dispersing 18.5 mg of composite catalyst in 25 mL of ethanol/water solution (75/25 volumetric ratio). A solution of a 5 wt% Nafion (100 μL) was added to the ink as a proton conducting binder to ensure good adhesion onto the electrode. The catalyst ink was dispersed by ultrasonification for 30 min. The dispersion was dropped onto a 6 mm diameter glassy carbon electrode using a micropipette. the glassy carbon surface was previously buff polished using a suspension of 0.3 then 0.05 μm alumina. The amount of Pt on the electrode was fixed at a loading of 17.3 (μg-Pt) cm^{-2}, regardless of the RuO_2ns content.

Electrochemical measurements.— Hydrodynamic voltammograms were recorded with a rotating disk electrode (Nikko Keisoku) in a standard three electrode electrochemical cell. Carbon fiber (Toho Tenax Co., HTA-3K) and a reversible hydrogen electrode (RHE) were used as the counter and reference electrodes, respectively. Electrochemical experiments were performed in 0.5 M H_2SO_4 electrolyte. Initial cleaning of the electrocatalyst surface was conducted by cycling

*Electrochemical Society Active Member.
zE-mail: wsugi@shinshu-u.ac.jp

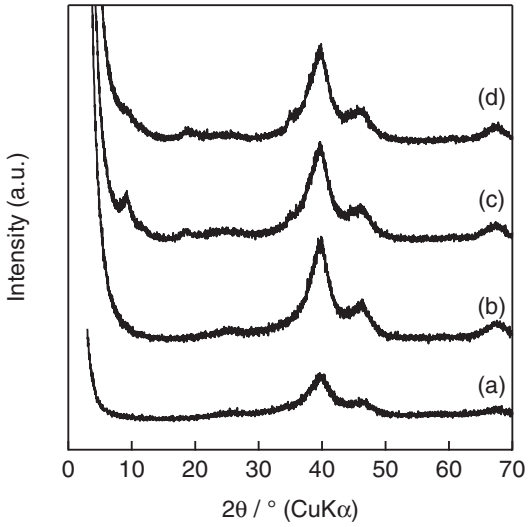

Figure 1. The XRD patterns of (a) Pt/C, (b) RuO_2ns(0.05)-Pt/C, (c) RuO_2ns(0.3)-Pt/C and (d) RuO_2ns(0.5)-Pt/C.

between 0.05–1.2 V vs. RHE at 50 mV s^{-1} for 30 cycles at 25°C under N_2 bubbling. Linear sweep voltammetry in N_2-purged, de-aerated 0.5 M H_2SO_4 electrolyte was first recorded at 10 mV s^{-1} from 0.05 to 1.2 V vs. RHE (anodic scan) at rotating rates of $\omega = 2200$, 1600, 1200, 800, and 400 rpm at 60°C. Three cycles were performed between 0.05–0.9 V vs. RHE at 50 mV s^{-1} to measure the electrochemically active surface area (ECSA) of Pt at 60°C. ECSA was estimated by integration of the hydrogen desorption charge by integration of the cyclic voltammogram from 0.05 V vs. RHE to 0.4 V vs. RHE and the Coulombic charge necessary for oxidation as 210 μC cm^{-2}. ECSA of RuO_2ns(*n*)-Pt/C was estimated after subtraction of the overlapping redox peaks due to RuO_2ns in the hydrogen desorption region. ORR was characterized by linear sweep voltammetry in O_2 saturated 0.5 M H_2SO_4 from 0.05 to 1.2 V vs. RHE (anodic scan) at 10 mV s^{-1} at the respective rotating rates. The LSV data collected in de-aerated electrolyte was used as background and subtracted from the data recorded in O_2-saturated 0.5 M H_2SO_4. Kinetically controlled current, i_k, was obtained with Koutecky-Levich plots (i.e., plots of the inverse of observed current, i^{-1} vs. $\omega^{-1/2}$) by extrapolating the regression lines on the plots to the *y* intercept. Kinetically controlled current density (j_k, mass activity) was calculated by dividing i_k with the mass of Pt.

Accelerated durability tests (ADT) were conducted by performing 50 cycles between 0.6–1.2 V vs. RHE at 100 mV s^{-1} in O_2 saturated 0.5 M H_2SO_4 (60°C) at 1600 rpm. LSV in N_2 and O_2 were measured again to obtain the ORR activity of the degraded electrocatalysts.

Results and Discussion

Figure 1 shows the XRD patterns of the electrocatalysts. The XRD peaks attributed to metallic Pt in RuO_2ns(*n*)-Pt/C are identical in peak position and width with Pt/C, suggesting that Pt is not affected by the mixing treatment with RuO_2ns. The Pt particle size calculated based on the Scherrer equation was 3.5 nm for all electrocatalysts. The diffraction peaks that may be attributed to tetrabutylammonium-$RuO_{2.1}$ or the layered $H_{0.2}RuO_{2.1}$[29] are not evident for composites with low RuO_2ns content. For composite catalyst with higher RuO_2ns content, weak diffraction peaks at $2\theta = 9.2°$ ($d = 0.98$ nm) and $2\theta = 18.2°$ ($d = 0.48$ nm) corresponding to the (002) and (003) diffraction peaks of the tetrabutylammonium-$RuO_{2.1}$ intercalation compound[29] were observed, suggesting partial agglomeration (re-stacking) of RuO_2ns. During the preparation of RuO_2ns-Pt/C composite with RuO_2/Pt = 0.05, 0.1 and 0.2, the solution becomes clear after sedimentation, which means that all of the RuO_2ns have reacted with Pt/C. On the other hand, for higher amount of RuO_2ns, the solution is slightly brown, indicating that excess RuO_2ns cannot form a composite with Pt/C, and re-stacks.

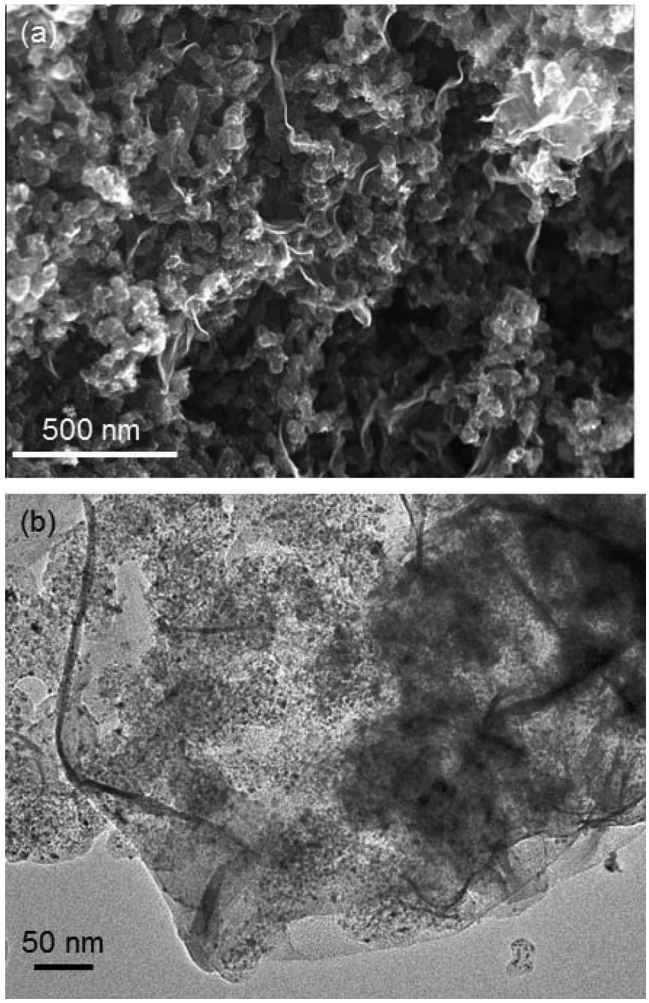

Figure 2. A typical (a) SEM image and (b) TEM image of RuO_2ns(0.3)-Pt/C.

Typical SEM and TEM images of RuO_2ns(0.3)-Pt/C are given in Figure 2. RuO_2ns with lateral size of a few hundred nanometers is homogeneously mixed with Pt/C, complementing the XRD results. Figure 3 shows the particle size distribution of Pt in Pt/C and RuO_2ns(0.3)-Pt/C electrocatalysts. The mean diameter (3.2 nm) and the distribution are identical for both electrocatalysts and is concordant with the XRD results. XRD, SEM and TEM data show that the structure, particle size and distribution are not affected by the preparation method. Thus, it can be said that RuO_2ns are microscopically intimately mixed with Pt/C, although slight aggregation of RuO_2ns occurs at higher loadings.

Figure 4 show typical cyclic voltammograms in de-aerated 0.5 M H_2SO_4 at 60°C. Redox peaks characteristic of RuO_2ns (shown with asterisks) are observed, which progressively increases as a function of RuO_2ns content (inset). The redox peaks between 0.45 and 0.70 V vs. RHE are due to adsorption-desorption of ionic species on the surface of RuO_2ns.[30,34–36] The peak at 0.11 V vs. RHE is characteristic of a monolayer of RuO_2 nanosheet in H_2SO_4 and may be due to adsorption-desorption of anionic species (HSO_4^- or SO_4^{2-}) on the surface of RuO_2ns.[29,37] The ECSA for Pt/C was 55 m^2 (g-Pt)$^{-1}$. The ECSA for RuO_2ns(*n*)-Pt/C are slightly higher than pristine Pt/C (Table I).

Figure 5 shows the linear sweep voltammograms at 1600 rpm of fresh Pt/C, RuO_2ns(0.1)-Pt/C, RuO_2ns(0.3)-Pt/C and RuO_2ns(0.5)-Pt/C electrocatalysts. Koutecky-Levich plots at 0.9 V vs. RHE are shown in Figure 6. The initial mass specific kinetic current density

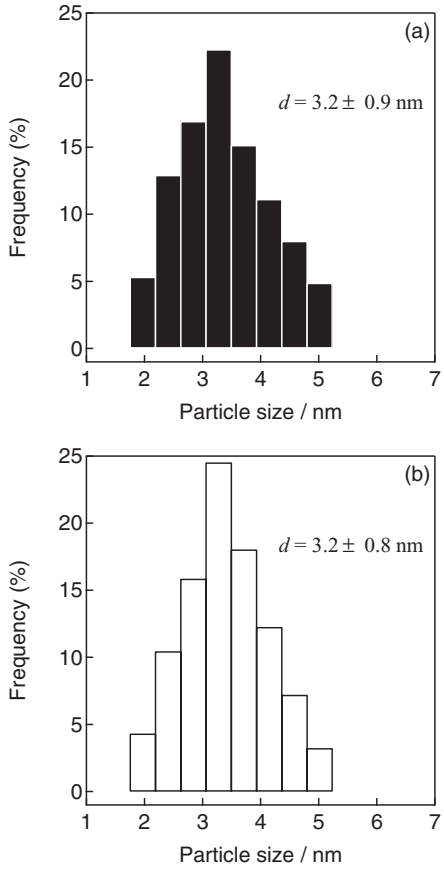

Figure 3. Pt particle size distribution for (a) Pt/C and (b) RuO_2ns(0.3)-Pt/C.

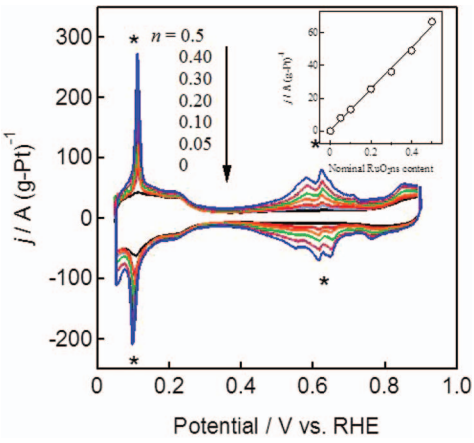

Figure 4. Cyclic voltammograms of RuO_2ns(n)-Pt/C, with $n = 0$ to 0.5 at 50 mV s^{-1} in 0.5 M H_2SO_4(60°C).

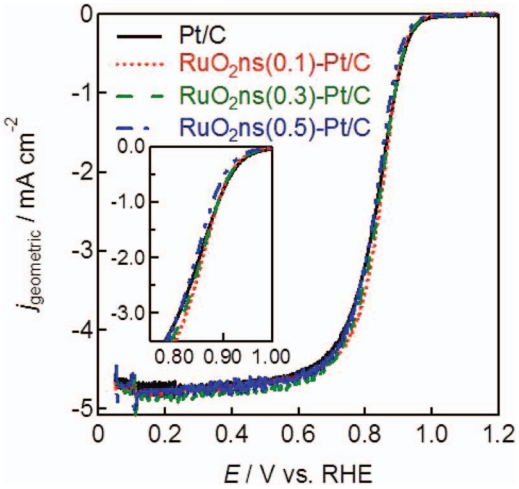

Figure 5. Linear sweep voltammograms of RuO_2ns(n)-Pt/C, with $n = 0$, 0.1, 0.3 and 0.5 at $\omega = 1600$ rpm, $\nu = 10$ mV s^{-1} in 0.5 M H_2SO_4(60°C).

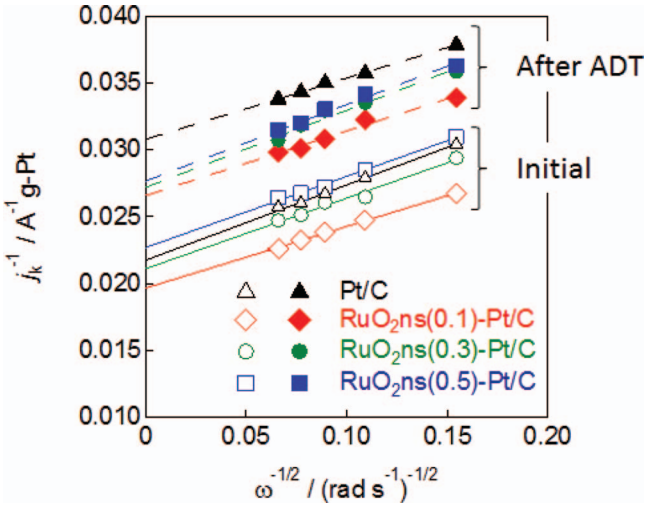

Figure 6. Koutecky-Levich plots of Pt/C and RuO_2ns-Pt/C before (open markers and after durability test (filled markers) at 0.90 V vs. RHE.

j_k at 0.9 V vs. RHE of Pt/C electrocatalyst was 45 A $(g\text{-Pt})^{-1}$. An increase in initial activity of 20% was observed for RuO_2ns(0.05)-Pt/C (Figure 7). Increasing loading results in a continuous decrease in mass activity, and the RuO_2ns(0.4)-Pt/C electrocatalyst shows activity comparable to pristine Pt/C. The reason for the volcano-type behavior can be interpreted as the competition between increased available Pt sites for ORR with addition of RuO_2ns and obstruction of O_2 diffusion at high RuO_2ns loading.

The Koutecky-Levich plots obtained after ADT for Pt/C, RuO_2ns(0.1)-Pt/C RuO_2ns(0.3)-Pt/C RuO_2ns(0.5)-Pt/C are given in

Table I. Composition, initial ECSA, and ECSA after ADT of catalysts.

Sample	Composition / mass%			ECSA / m^2 $(g\text{-Pt})^{-1}$		
	RuO_2	Pt	C	Initial	After ADT	Retention of ECSA (%)
Pt/C	-	46.1	53.9	55	39	71
RuO_2ns(0.05)-Pt/C	1.5	45.4	53.1	65	47	72
RuO_2ns(0.1)-Pt/C	3	44.7	52.3	57	40	70
RuO_2ns(0.2)-Pt/C	5.9	43.4	50.7	57	43	75
RuO_2ns(0.3)-Pt/C	8.6	42.1	49.3	62	46	74
RuO_2ns(0.4)-Pt/C	11.2	40.9	47.9	63	47	75
RuO_2ns(0.5)-Pt/C	13.6	39.8	46.6	68	53	78

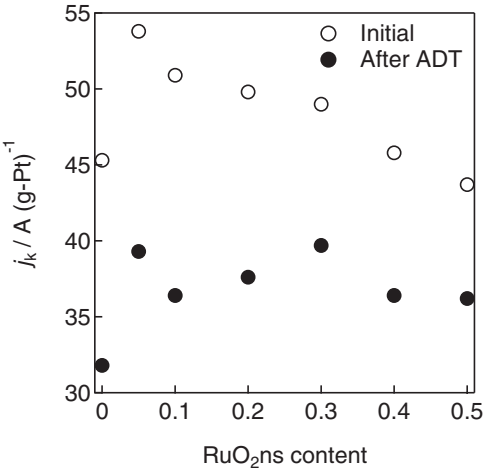

Figure 7. Mass activity before and after accelerated durability test as a function of the RuO_2ns content.

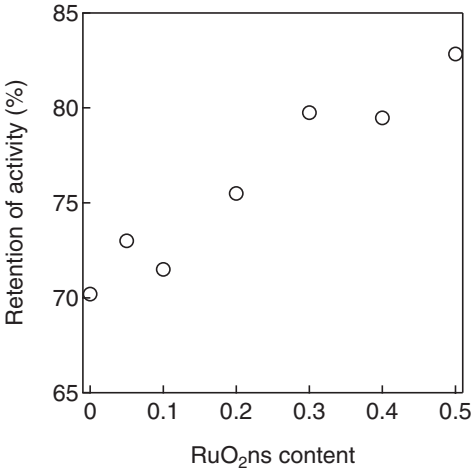

Figure 8. Retention of activity after accelerated durability test as a function of the RuO_2ns content.

Figure 6. The mass specific kinetic current j_k at 0.9 V vs. RHE for ORR after ADT are shown in Figure 7. The retention rate, which is the j_k after ADT divided by the initial j_k, is plotted as a function of the RuO_2ns content in Figure 8. The activity of Pt/C at 0.9 V vs. RHE decreases to 31 A (g-Pt)$^{-1}$ after ADT, *i.e.* retention of activity was 70%. The retention of mass activity continuously increase with increasing RuO_2ns content, up to 83% for RuO_2ns(0.5)-Pt/C. The RuO_2ns(0.3)-Pt/C shows the highest mass activity after ADT of 39 A (g-Pt)$^{-1}$. Table I summarizes the ECSA after ADT and the retention of ECSA. The trend in the retention rate of ECSA and j_k are similar. The loss of ECSA is smaller and the retention is higher for electrocatalysts containing RuO_2ns with RuO_2ns(0.5)-Pt/C electrocatalyst exhibiting the highest ECSA and ECSA retention.

Figure 9 shows the TEM images of Pt/C and RuO_2ns(0.3)-Pt/C electrocatalysts after ADT and also the size distribution of Pt

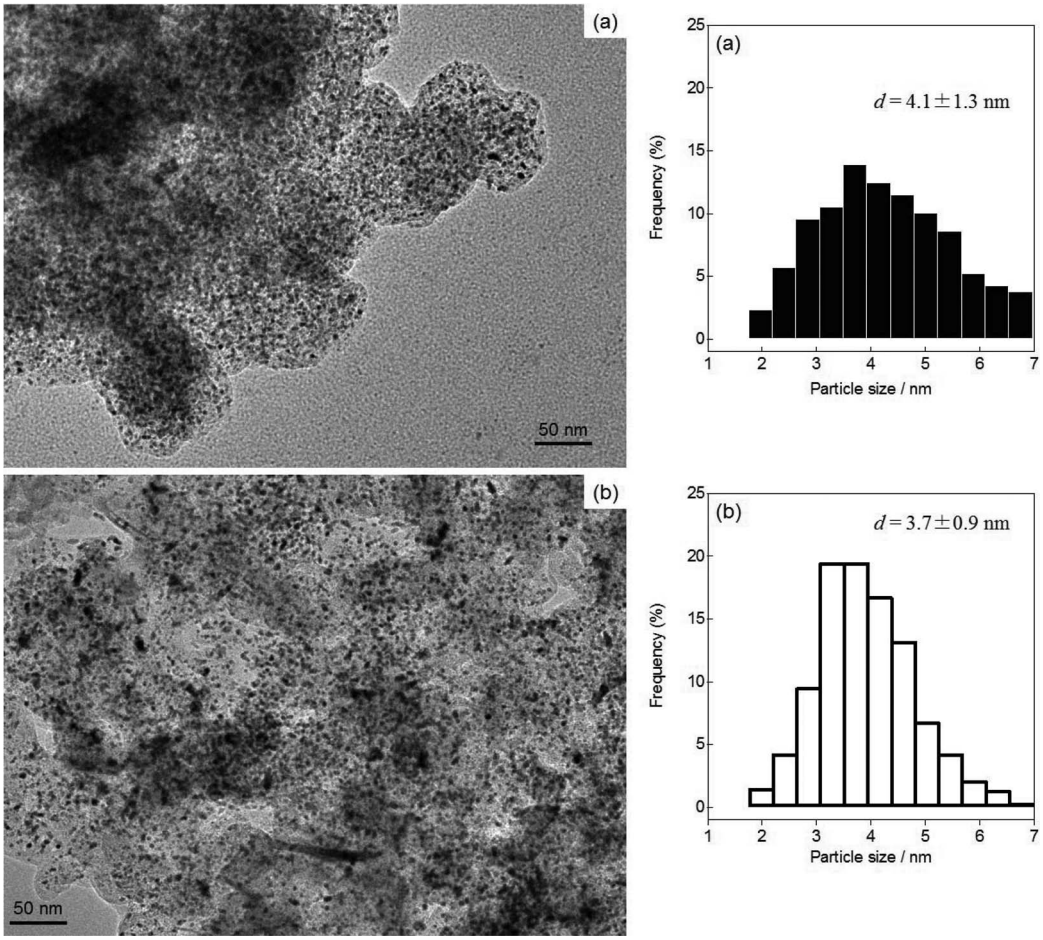

Figure 9. TEM images and Pt particle size distribution (a) Pt/C and (b) RuO_2ns(0.3)-Pt/C composite catalyst after accelerated durability test.

particles obtained from multiple TEM images. The mean Pt particle size after ADT was 4.1 ± 1.3 nm for Pt/C and 3.7 ± 0.9 nm for RuO_2ns(0.3)-Pt/C. The smaller particle size and narrower distribution for RuO_2ns(0.3)-Pt/C suggests suppression of Pt dissolution and/or sintering.

Based on the obtained results, the reason for enhanced catalyst durability is discussed. DFT studies have shown that Pt atoms strongly adsorb on RuO_2, resulting in a transfer of electron density from Pt to RuO_2.[38] In the case of RuO_2ns-Pt/C electrocatalyst, as RuO_2ns is simply nearby Pt, the interaction between Pt and RuO_2 may be weaker, however if the interaction is strong enough, a change in the *d*-band center of Pt may be possible. The interaction between the RuO_2ns and dissolved cationic Pt species obstructing the diffusion of Pt ions may be another possibility. Negatively charged RuO_2ns[28] may act as a trapping site for cationic Pt^{n+} which has been suggested as the dissolution species of Pt.[39] In fact, model electrode studies with RuO_2ns/HOPG has revealed a strong chemical interaction between RuO_2ns and dissolved Pt species as well as between RuO_2ns and metallic Pt.[40,41] In situ studies shows that dissolved Pt species specifically adsorb on RuO_2ns and not on HOPG.[40] Also, Pt deposited by vacuum deposition on RuO_2ns and HOPG is more stable during cyclic voltammetry on nanosheet support rather than HOPG.[41]

Conclusions

Composite electrocatalysts of Pt/C and RuO_2 nanosheet (RuO_2ns) derived from layered $K_{0.2}RuO_{2.1} \cdot nH_2O$ exhibit higher activity and durability than pristine Pt/C toward oxygen reduction reaction. Composite electrocatalysts with lower RuO_2ns content provide higher activity, while higher amount leads to better durability. The initial mass activity shows a maximum as a function of the RuO_2ns content, with $RuO_2/Pt = 0.05$ showing a 20% increase (54 A $(g\text{-}Pt)^{-1}$) compared to pristine Pt/C (45 A $(g\text{-}Pt)^{-1}$). A clear difference in long term durability was observed when potential cycling in O_2. After accelerated durability test, the composite catalyst with $RuO_2/Pt = 0.3$ exhibits ORR activity of 39 A $(g\text{-}Pt)^{-1}$, which is 25% higher than pristine Pt/C electrocatalyst. The increase in particle size is suppressed for the RuO_2ns-Pt/C composite catalysts suggesting a lower degradation of the composite catalysts compared to pristine Pt/C. The results obtained in this work suggest that RuO_2 nanosheet functions as a stabilizer for platinum based electrocatalyst.

Acknowledgments

This work was supported in part by the "Polymer Electrolyte Fuel Cell Program" from the New Energy and Industrial Technology Development Organization (NEDO) of Japan.

References

1. X. Li, S. Park, and B. Popov, *J. Power Sources*, **195**, 445 (2010).
2. V. Jalan and E. J. Taylor, *J. Electrochem. Soc.*, **130**, 2299 (1983).
3. B. C. Beard and P. N. Ross, *J. Electrochem. Soc.*, **137**, 3368 (1990).
4. S. Mukerjee and S. Srinivasan, *J. Electroanal. Chem.*, **357**, 201 (1993).
5. T. Toda, H. Igarashi, H. Uchida, and M. Watanabe, *J. Electrochem. Soc.*, **146**, 3750 (1999).
6. V. Stamenkovic, B. Mun, M. Arenz, K. Mayrhoffer, C. Lucas, G. Wang, P. Ross, and N. Markovic, *Nat. Mater.*, **6**, 241 (2007).
7. S. Zignani, E. Antolini, and E. Gonzalez, *J. Power Sources*, **191**, 344 (2009).
8. K. Jayasayee, J. A. R van Veen, T. G. Manivasagam, S. Celebi, E. J. M. Hensen, and F. A. de Bruijn, *Appl. Catal. B-Environ*, **111–112**, 515 (2012).
9. J. Zheng, R. Fu, T. Tian, X. Wang, and J. Ma, *Int. J. Hydrogen Energy*, **37**, 12994 (2012).
10. K. Neyerlin, R. Srivastaya, C. Yu, and P. Strasser, *J. Power Sources*, **186**, 261 (2009).
11. S. Koh, M. Toney, and P. Strasser, *Electrochim. Acta*, **52**, 2765 (2007).
12. N. M. Markovic, T. J. Schmidt, V. Stamenkovic, and P. N. Ross, *Fuel Cells*, **2**, 105 (2001).
13. N. Honick, M. Zorko, M. Bele, S. Hocevar, and M. Gaberscek, *J. Phys. Chem. C*, **116**, 21326 (2012).
14. H. R. Colon-Mercado and B. N. Popov, *J. Power Sources*, **155**, 253 (2006).
15. O. A. Baturina, Y. Garsany, T. J. Zega, R. M. Stroud, T. Schull, and K. Swider-Lyons, *J. Electrochem. Soc.*, **155**, B1314 (2008).
16. P. J. Bouwman, W. Dmowski, J. Stanley, G. B. Cotten, and K. Swider-Lyons, *J. Electrochem. Soc.*, **151**, A1989 (2004).
17. R. N. Lakshmi and K. S. Dhathathreyan, *Int. J. Hydrogen Energy*, **33**, 7521 (2006).
18. A. Masao, S. Noda, F. Takasaki, K. Ito, and K. Sasaki, *Electrochem. Solid-State Lett.*, **12**, B119 (2009).
19. S. Vino Selvaganesh, G. Selvarani, P. Sridhar, S. Pitchumani, and A. K. Shukla, *J. Electrochem. Soc.*, **159**, B463 (2012).
20. C. Lo, G. Wang, A. Kumar, and V. Ramani, *Appl. Catal. B-Environ.*, **140–141**, 133 (2013).
21. J. P. Zheng and T. R. Jow, *J. Electrochem. Soc.*, **142**, L6 (1995).
22. W. Sugimoto, H. Iwata, Y. Yasunaga, Y. Murakami, and Y. Takasu, *Angew. Chem. Int. Ed.*, **42**, 4092 (2003).
23. Q. Zeng, L. Zheng, J. Zeng, and S. Liao, *J. Power Sources*, **205**, 201 (2012).
24. X. Wu, H. Xu, L. Lu, J. Fu, and H. Zhao, *Int. J. Hydrogen Energy*, **35**, 2127 (2010).
25. L. Lu, H. Xu, H. Zhao, X. Sun, Y. Dong, and R. Ren, *J. Power Sources*, **242**, 99 (2013).
26. R. Srivastava and P. Strasser, *ECS Trans.*, **25**(1), 565 (2009).
27. V. Ho, N. Nguyen, C. Pan, J. Cheng, J. Rick, W. Su, J. Lee, H. Sheu, and B. Hwang, *Nano Energy*, **1**, 687 (2010).
28. K. Fukuda, H. Kato, J. Sato, W. Sugimoto, and Y. Takasu, *J. Solid State Chem.*, **182**, 2997 (2009).
29. T. Saida, W. Sugimoto, and Y. Takasu, *Electrochim. Acta*, **55**, 857 (2010).
30. W. Sugimoto, T. Saida, and Y. Takasu, *Electrochem. Commun.*, **8**, 411 (2006).
31. C. Chauvin, Q. Liu, T. Saida, K. Lokesh, T. Sakai, and W. Sugimoto, *ECS Trans.*, **50**(2), 1583 (2013).
32. D. Takimoto, C. Chauvin, and W. Sugimoto, *Electrochem. Commun.*, **33**, 123 (2013).
33. C. Wang, N. Markovic, and V. Stamenkovic, *ACS Catal.*, **2**, 891 (2012).
34. Y. Takasu, T. Fujiwara, Y. Murakami, K. Sasaki, M. Oguri, T. Asaki, and W. Sugimoto, *J. Electrochem. Soc.*, **147**, 4421 (2000).
35. Y. Takasu, H. Itaya, T. Kawaguchi, W. Sugimoto, and Y. Murakami, *Stud. Surf. Sci. Catal.*, **145**, 279 (2003).
36. W. Sugimoto, H. Iwata, Y. Yasunaga, Y. Murakami, and Y. Takasu, *J. Electrochem. Soc.*, **151**, A1181 (2004).
37. T. E. Lister, Y. Chu, W. Cullen, H. You, R. M. Yonco, J. F. Mithchell, and Z. Nagy, *J. Electroanal. Chem.*, **524–525**, 201 (2002).
38. P. Liu, J. T. Muckerman, and R. R. Adzic, *J. Chem. Phys.*, **124**, 141101-1 (2006).
39. P. J. Ferreira, Y. Shao-Horn, D. Morgan, R. Makharia, S. Kocha, and H. A. Gasteiger, *J. Electrochem. Soc.*, **152**, A2256 (2005).
40. Q. Liu, K. S. Lokesh, C. Chauvin, and W. Sugimoto, *J. Electrochem. Soc.*, **161**, F259 (2014).
41. Q. Liu, C. Chauvin, and W. Sugimoto, *submitted*.